Sinusoidal Output Current Implementation of DFIG Using Repetitive Control Under a Generalized Harmonic Power Grid With Frequency Deviation

Yipeng Song, *Student Member, IEEE*, and Heng Nian, *Senior Member, IEEE*

***Abstract*—The paper presents the control strategy of stator current harmonic distortion performance improvement for doubly fed induction generator (DFIG) using bandwidth-based repetitive control (BRC) under generalized harmonic grid voltage. The control target is to eliminate the DFIG stator current $6n \pm 1$ harmonic components; thus, sinusoidal stator output current can be injected into the power grid. Considering that the frequency deviation always occurs in the practical grid, the BRC regulator is designed on the basis of conventional repetitive control regulator with the introduction of control bandwidth. The closed-loop operation stability considering different bandwidth and gain parameter is also analyzed. Finally, the availability of the proposed BRC control strategy under generalized harmonic grid voltage is verified by experimental results.**

***Index Terms*—Bandwidth-based repetitive control (BRC), closed-loop operation stability, doubly fed induction generator (DFIG), generalized harmonic grid voltage.**

I. Introduction

THE harmonic distorted grid condition will severely deteriorate the output power quality of the renewable energy generation system. Especially for the doubly fed induction generator (DFIG)-based wind power generation system whose stator winding is directly connected to the power grid, the adverse stator current distortion, instantaneous active and reactive power pulsation and electromagnetic torque pulsation would occur as a consequence [1]–[3].

Up to now, several control strategies of the DFIG system under grid voltage distortion have been investigated in [3]–[9] with vector-oriented control or direct power control strategy; these works aimed at keeping stator or rotor current sinusoidal, or smooth active and reactive output power, or smooth electromagnetic torque. However, only the low-order fifth and seventh harmonic components of grid voltage were considered in the previous works [3]–[9].

Nowadays, the renewable power generation system has been widely applied in the weak grid, microgrid, or stand-alone power grid. The nonlinear load would inject harmonic distorted current into the grid, and the distorted current may include both low-order (fifth and seventh) and high-order harmonic (11th, 13th, 17th, 19th, etc.) components [10]. Since the microgrid or weak grid would always have line impedance that cannot be ignored, the harmonic distorted current would inevitably cause the harmonic voltage distortion on the point of common coupling (PCC), and the PCC voltage distortion will also contain the low-order and high-order harmonic components [10]. As a consequence, the DFIG operation and output power quality would be severely jeopardized if no effective control strategy considering the grid voltage harmonic components is implemented, and the grid voltage distortion condition would be further aggravated as well.

The proportional-integral resonant (PIR) regulator [3]–[7], [9] or vector proportional integral (VPI) resonant regulator [8] tuned at 300, 600, 900 Hz, etc., in the synchronous rotating frame, can be used to restrain the stator current harmonic components. Nevertheless, when the high-order harmonic voltage is taken into consideration for DFIG control, the complex control scheme configuration with more resonant regulators working in parallel has to be implemented, and large amount of DSP computation time would be consumed. Furthermore, the proper discretization method has to be carefully chosen to make sure that the resonant frequency of PIR and VPI regulators in the discrete domain would match precisely as that in the continuous domain, and the delay compensation should also be carefully considered [11]. Thus, the resonant regulator is inappropriate to implement the effective suppression of the stator current low- and high-order harmonic components simultaneously.

It has been reported that the repetitive control (RC) regulator is able to mitigate the $6n \pm 1$ harmonic current components [12]. Compared with the conventional resonant regulator, the simple control structure and less DSP computation burden, as well as the better steady-state performance of RC regulator can be guaranteed [12]–[21]. The RC regulator for three-phase grid-connected inverter was employed in [12] to eliminate the $6n \pm 1$ harmonic components of output current, in which $Q(z)$ was proposed to compensate the nonintegral ratio of sample frequency to the $6n$-order harmonic frequency. The RC strategy of DFIG operating in stand-alone mode was investigated in [13] to mitigate the harmonic distortion or unbalance in the stator terminal voltage. The dual mode-structure RC, which comprises two paralleled periodic signal generators, an odd harmonic one and an even harmonic one, was proposed in [14] to improve the control performance of RC with faster error convergence rate. A cascaded current–voltage control strategy for inverters using $H\infty$ repetitive controller was investigated in [15] to simultaneously

Manuscript received June 26, 2014; revised October 4, 2014 and November 19, 2014; accepted January 6, 2015. Date of publication January 12, 2015; date of current version August 21, 2015. Recommended for publication by Associate Editor M. Molinas.

The authors are with the College of Electrical Engineering, Zhejiang University, Hangzhou 310027, China (e-mail: eedqgcsyp@126.com; nianheng@zju.edu.cn).

Color versions of one or more of the figures in this paper are available online at http://ieeexplore.ieee.org.

Digital Object Identifier 10.1109/TPEL.2015.2390213

improve the power quality of the load voltage and current exchanged with the grid. The advanced current control strategy for distributed generations to transfer a sinusoidal current into the utility grid under the distorted grid voltage and nonlinear local load conditions was introduced in [16], and the PI controller and RC is adopted in the synchronous reference frame. The design of robust RC with time-varying sampling periods was reported in [17] to design a low-order, stable, robust, and causal IIR repetitive compensator using an optimization method to achieve fast convergence and high tracking accuracy. A generic digital $nk \pm m$-order harmonic repetitive control ($nk \pm m\mathrm{RC}$) scheme was presented in [18] for constant-voltage constant-frequency pulse width modulation (PWM) converters to track/remove any $nk \pm m$-order harmonic frequencies efficiently. A multirate RC scheme was developed and applied to constant-voltage constant frequency PWM converter systems in [19]. The inherent relationship between RC and resonant control was comprehensively developed in [20], in which the partial equivalence between RC regulator and resonant regulator, the advantages and disadvantages of multiresonant over RC is pointed out. A general parallel structure RC scheme for multiphase dc–ac PWM converters to cancel output total harmonic distortion more efficiently was developed in [21].

Meanwhile, the grid frequency is allowed to vary within the range of 49.8 and 50.2 Hz in the practical situation [22]. Unfortunately, the conventional RC regulator, which can be expressed as the sum of series of ideal resonant regulators [20], has quite precipitous magnitude response and phase response at the adjacent of the control frequency (300, 600, 900 Hz, etc.) due to the absence of the resonant bandwidth parameter [11]. When the grid frequency deviation happens, the resonant regulator usually employs the parameter of resonant bandwidth to enlarge the magnitude response near the resonant frequency point [3]–[9]; thus, the stronger robustness of the resonant regulator against grid frequency deviation can be guaranteed. Nevertheless, the series of ideal resonant regulators included in the conventional RC regulator do not have the resonant bandwidth parameter; thus, the DFIG stator current harmonic suppression capability based on conventional RC regulator would be severely deteriorated when grid frequency deviation happens. Therefore, for the purpose of improving DFIG operation performance in practical application, the control robustness of conventional RC regulator against grid frequency deviation should be improved.

In order to improve the control robustness of conventional RC regulator against grid frequency deviation, an improved RC scheme with a special designed finite-impulse response (FIR) filter was proposed in [23]; the FIR filter can be adjusted according to the varied grid frequency and maintain its resonant frequencies matching the grid fundamental and harmonic ones. However, the design of the FIR filter is complicated since several parameters of FIR filter need to be carefully selected under grid frequency variation. Moreover, the introduction of FIR filter would also increase the control system complexity.

Since the resonant bandwidths of PIR and VPI regulators are always introduced to improve their control robustness against grid frequency deviation [3]–[9], the similar bandwidth design method can be employed on the basis of conventional RC regulator, and its regulation capability would be improved when the DFIG stator current harmonic components deviate from the normal 300, 600, and 900 Hz. Compared with [23], the proposed bandwidth-based RC (BRC) regulator has the advantage of simple structure and easy implementation; only one parameter of bandwidth needs to be determined and flexibly adjusted under the different situation of grid frequency deviation.

This paper investigates the BRC strategy for DFIG under the generalized harmonic grid voltage to achieve the sinusoidal stator current injected into the power grid. This paper is organized in following manner. In Section II, the mathematical model of DFIG under the generalized harmonic voltage is briefly mentioned as a foundation. The proposed BRC strategy is described in detail in Section III. In Section IV, the shortcoming of conventional RC regulator, the design method of the proposed BRC regulator, as well as the analysis of closed-loop stability considering different bandwidth and gain parameter, is discussed. Finally, in Section V, the experimental system based on 1 kW laboratory DFIG is developed to validate the availability of the proposed BRC strategy.

II. Mathematical Model of DFIG Under Generalized Harmonic Voltage

The mathematical modeling of DFIG under fifth and seventh distorted grid voltage has been well established in [3], and the similar deduction can be accomplished when the $6n \pm 1$-order harmonic components of grid voltage is considered.

When DFIG works under the generalized harmonic voltage, the stator current would also contain both low- and high-order harmonic sequences due to the stator's winding direct connection to the power grid; thus, the stator current can be presented as follows:

$$I^{+}_{\mathrm{sdq}} = I^{+}_{\mathrm{sdq}+} + \sum_{n=1}^{\infty} \left(I^{(6n-1)-}_{\mathrm{sdq}(6n-1)-} e^{-j6n\theta_1} + I^{(6n+1)+}_{\mathrm{sdq}(6n+1)+} e^{j6n\theta_1} \right) \quad (1)$$

where I is current; subscripts d, q represent d-axis and q-axis components; subscripts s represent stator components of DFIG; superscripts $+$, $(6n-1)-$ and $(6n+1)+$ represent the reference frames rotating at the fundamental angular speed in the positive direction, at the angular speed of $(6n-1)$ times of fundamental angular speed in the negative direction, and at the angular speed of $(6n+1)$ times of fundamental angular speed in the positive direction; subscripts $+$, $(6n-1)-$ and $(6n+1)+$ represent the fundamental and harmonic components, i.e., 5th, 7th, 11th, 13th, 17th, 19th, etc. θ_1 represents the phase angle of grid voltage fundamental component.

Therefore, based on (1), it can be found out that, due to the harmonic distorted grid voltage, the stator current of DFIG would contain the harmonic components of $5-$, $7+$, $11-$, $13+$, $17-$, $19+$, etc., sequence in the stationary frame, these components would behave as 6–, 6+, 12–, 12+, 18–, 18+, etc., times of grid voltage fundamental frequency in the $(dq)^{+}$ synchronous frame. In order to enhance the output power quality of DFIG under the

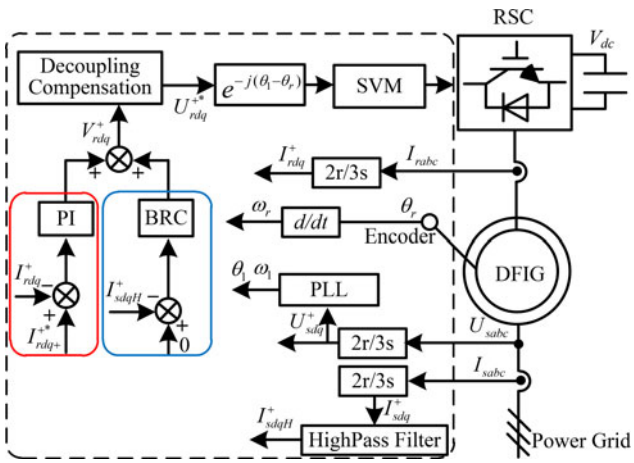

Fig. 1. Block diagram of the proposed stator current harmonic suppression strategy.

harmonic distorted grid voltage, the control target is selected to output the sinusoidal stator current into the power grid.

III. Stator Current Harmonic Suppression Strategy

For the purpose of removing the stator harmonic current components under the generalized harmonic voltage, the BRC regulator is employed for DFIG control in this paper. Fig. 1 shows the control block diagram of the proposed stator current harmonic suppression strategy, which is almost similar to the control scheme in [9]. Since only the fifth- and seventh-order harmonic components of grid voltage was considered in [9], the resonant regulator is sufficient to deal with the stator current fifth and seventh harmonic sequence. However, since more harmonic sequences need to be considered in this paper, the RC strategy is employed in the proposed control strategy for DFIG under the generalized harmonic voltage. Furthermore, it can be seen that no harmonic sequence extraction of grid voltage or stator current is required; this would simplify the complexity of the proposed control strategy and reduce the DSP computation burden.

As can be seen from Fig. 1, the distorted grid voltage $U_{\rm sabc}$ would be sampled and transformed to the synchronous $(dq)^+$ frame as $U^+_{\rm sdq}$, and the phase-locked loop module integrated with low-pass filter can be used to obtain the phase angle information of voltage fundamental frequency component. The rotor speed ω_r and position angle θ_r can be obtained by the encoder output. The stator current $I_{\rm sabc}$ and rotor current $I_{\rm rabc}$ are transformed to $(dq)^+$ frame as $I^+_{\rm sdq}$ and $I^+_{\rm rdq}$, respectively, which would be used in the two separate current closed-loop control. The two current closed-loop control is elaborated as follows.

1) The PI regulator is used to control the fundamental component of rotor current. The rotor current fundamental component reference $I^{+*}_{\rm rdq+}$ can be obtained according to the output active and reactive power reference based on maximum power point track (MPPT) and reactive power compensation command [3]. Normally, MPPT in the wind turbine system is used to generate the output power reference signals based on the wind speed, grid operation requirement, etc. The rotor current reference corresponding to the power reference is sent to the converter; the error of rotor current can be obtained by comparing the actual rotor current $I^+_{\rm rdq}$ and reference $I^{+*}_{\rm rdq+}$, and the PI current controller is adopted to make sure that the DFIG actual output power would follow precisely the power reference generated by MPPT. Since the rotor current control is implemented in $(dq)^+$ synchronous rotating frame, the rotor current control error would always contain dc component and $6n$-order ac signal components. The dc component can be restrained to zero by PI regulator, while the $6n$-order ac error signals can be automatically neglected due to the limited ac signal tracking capability of the PI regulator. Thus, it can be found out that the closed-loop PI control of rotor current is unable to eliminate the stator current distortion; thus, the additional closed-loop control of stator current with BRC regulator needs to be introduced.
2) The BRC regulator is used to directly suppress the harmonic components of stator current. As shown in Fig. 1, the reference of BRC regulator is set as zero (meaning no harmonic components of stator current are expected to exist), and stator current feedback $I^+_{\rm sdq}$ would include both dc and $6n$ component of stator current. Due to that the dc component in error signal would unfortunately interfere the harmonic control capability of RC regulator [13], an additional high-pass filter is used to remove the dc component in the stator current feedback, as described in Section IV-C. It should be noted that the aforementioned process of stator current dc component removing with the adoption of high-pass filter can be considered as the stator current harmonic components extraction process. Several harmonic extraction methods are available, for instance, the multiple complex-coefficient filter is adopted in [3] to extract the fundamental, fifth harmonic sequence, and seventh harmonic sequence in the grid voltage. The decomposing scheme based on multiple second-order generalized integrators and a frequency-locked loop (MSOGI-FLL) is introduced in [4] and [5] to extract the grid voltage negative, fifth and seventh harmonic components. The band pass filter is also adopted to extract the fifth and seventh harmonic components in [6]. All these harmonic extraction methods are capable of extracting each harmonic sequence quickly and accurately. However, in this paper, the detailed information on each harmonic sequence of stator current is not required, but only the sum of entire harmonic sequences of stator current needs to be known; thus, for the sake of control system simplicity, only the high-pass filter is adopted to acquire the stator current harmonic components.

Therefore, two closed-loop current control output, together with the decoupling compensation item [3] as given in (2), would finally produce the rotor control reference voltage $U^{+*}_{\rm rdq}$. The reference voltage is then transformed to the rotor stationary frame, and the space vector modulation is used to obtain the switching signals

$$E^+_{\rm rdq} = \left(R_r I^+_{\rm rdq} + j\omega_1 \sigma L_r I^+_{\rm rdq}\right) + L_m \left(U^+_{\rm sdq} - R_s I^+_{\rm sdq} - j\omega_r \psi^+_{\rm sdq}\right)/L_s \quad (2)$$

where R_s and R_r are stator and rotor resistances, subscripts *r* represent rotor components of DFIG, ω_1 and ω_r are grid voltage angular speed and rotor angular speed, L_s, L_r are the stator and rotor inductance, $\sigma = 1 - L_m^2/L_sL_r$ is the leakage inductance coefficient, and L_m is the mutual inductance.

IV. Design and Analysis of BRC Regulator

For the purpose of eliminating DFIG stator current harmonic components under generalized harmonic grid voltage, as well as considering the fact that the grid voltage frequency is allowed to vary within the range of 49.8 and 50.2 Hz [22], the BRC regulator is proposed to improve the closed-loop control robustness against grid frequency deviation.

A. Shortcoming of the Conventional RC Regulator

According to [20], the conventional RC regulator in the continuous domain can be presented as follows:

$$G_{\mathrm{rc}s}(s) = k_{\mathrm{rc}}\frac{e^{-sT_0}}{1-e^{-sT_0}} \tag{3a}$$

where k_{rc} is the gain parameter of conventional RC regulator, T_0 is the period of fundamental control frequency, and $T_0 = 1/300\,\mathrm{s}$ in this paper since the stator current distortion includes harmonic components of 300, 600, 900 Hz, etc.

Moreover, based on the nature of exponential function, the conventional RC regulator given in (3a) can also be written as [20]

$$G_{rcs}(s) = -\frac{k_{\mathrm{rc}}}{2} + \frac{k_{\mathrm{rc}}}{T_0}\frac{1}{s} + \frac{2k_{\mathrm{rc}}}{T_0}\sum_{n=1}^{\infty}\frac{s}{s^2+\omega_n^2} \tag{3b}$$

where T_0 is the period of fundamental control frequency, which is the same as in (3a).

On the other hand, according to [12], the conventional RC regulator in the discrete domain can be presented as

$$G_{\mathrm{rc}z}(z) = k_{\mathrm{rc}}\frac{Q(z)z^{-N}}{1-Q(z)z^{-N}} \tag{4a}$$

$$Q(z) = (1-D) + Dz^{-1} \tag{4b}$$

where *D* is equal to the fractional part of $N_0/6$, and N_0 is the ratio of the sampling frequency to the grid fundamental frequency [12]. And the delay *N* is set to the integral part of $N_0/6$. It has been proved in [12] that the block $Q(z)z^{-N}$ is capable of maintaining the great RC performance when one-sixth of the ratio N_0 is noninteger.

It should be noted that both (3a), (3b), and (4a), (4b) can be used to describe the RC regulator in the different domain ((3a) and (3b) in the continuous domain and (4a) and (4b) in the discrete domain). Since the resonant regulator containing the resonant bandwidth ω_c [3]–[8] is always presented in the continuous domain, in order to more clearly and explicitly explain the proposed method of introducing the bandwidth parameter into the conventional RC regulator, the design procedure of BRC regulator is first illustrated on the basis of conventional RC regulator in the continuous domain in (3a) and (3b), and then would be transplanted to the RC regulator in the discrete domain in (4a) and (4b).

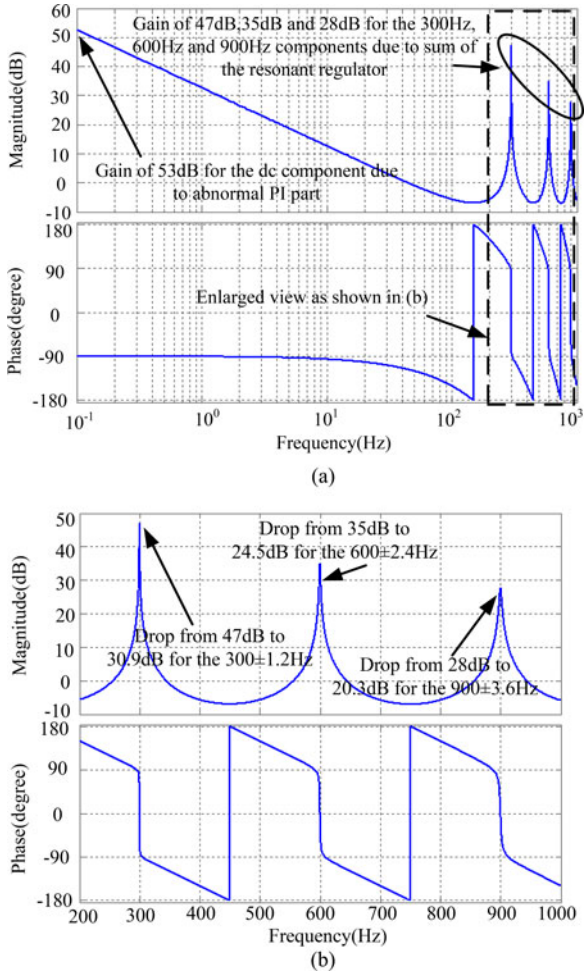

Fig. 2. Bode diagram of conventional RC regulator ($k_{\mathrm{rc}} = 0.9$, $Q(z) = 2/3 + 1/3^*z^{-1}$, and $N = 33$).

Fig. 2 gives out the bode diagram of conventional RC regulator as given in (4a) and (4b) with the $k_{\mathrm{rc}} = 0.9$, $Q(z) = 2/3 + 1/3^*z^{-1}$, and $N = 33$ according to [12] due to the sample frequency of 10k Hz and the fundamental control frequency of 300 Hz. It can be observed from (3a), (3b), (4a), (4b), and Fig. 2 that:

1) The conventional RC regulator in both continuous domain and discrete domain contains the abnormal PI part, namely "$-k_{\mathrm{rc}}/2 + k_{\mathrm{rc}}/T_0 s$." Since both the proportional parameter ($-k_{\mathrm{rc}}/2$) and integral part ($k_{\mathrm{rc}}/T_0 s$) are only determined by the RC gain parameter k_{rc}, the parameters of proportional part and integral part of RC regulator cannot be tuned independently, while the parameters of proportional part and integral part in the normal PI regulator can be adjusted independently. Additionally, both proportional part and integral part in the normal PI regulator have positive sign, while in RC regulator, the proportional part has negative sign "–" and the integral part has positive sign "+." Therefore, even high gain of 53 dB for the dc component can be obtained, this abnormal PI part would unfortunately

fail to regulate the stator current fundamental component, but interfere the normal operation of DFIG stator current regulation, which can be seen from Fig. 2(a).

2) Besides the abnormal PI part, the conventional RC regulator also contains series of resonant regulators in ideal expression, which are responsible for suppressing the stator current harmonic components because of the high magnitude response of 47, 35, and 28 dB at 300, 600, 900 Hz, etc., as can be seen from Fig. 2(b). However, the equivalent ideal resonant regulators lack the bandwidth parameters in the denominator; thus, when the grid frequency deviation of ± 0.2 Hz happens (that is ± 1.2 Hz for 300 Hz, ± 2.4 Hz for 600 Hz, ± 3.6 Hz for 900 Hz), the gain would drop from 47 to 30.9 dB for the 300 ± 1.2 Hz, 35 dB to 24.5 dB for the 600 ± 2.4 Hz, and 28 dB to 20.3 dB for the 900 ± 3.6 Hz. Therefore, the conventional RC regulator's robustness against grid frequency deviation would be degraded if no bandwidth parameter is introduced.

B. Proposed BRC Regulator Design

In order to improve the stator harmonic current suppression capability of DFIG, the robustness against grid frequency deviation of RC regulator should be enhanced. Based on the conventional RC regulator expression in the continuous domain as given in (3b), the bandwidth parameter can be easily introduced, which is similar as the introduction of bandwidth to the resonant regulators. Besides, the abnormal PI part can also be removed. Then, the BRC regulator with bandwidth parameter and without abnormal PI part in the discrete domain can be obtained.

According to (3b), the resonant parts in the conventional RC regulator can be extracted by removing the abnormal PI part as

$$\mathrm{RESO} = \frac{T_0}{2k_{\mathrm{rc}}}\left(G_{\mathrm{rcs}}(s) + \frac{k_{\mathrm{rc}}}{2} - \frac{k_{\mathrm{rc}}}{T_0}\frac{1}{s}\right) = \sum_{n=1}^{\infty}\frac{s}{s^2+\omega_n^2}. \tag{5}$$

It can be found that series of resonant regulators are included in (5), and each single resonant regulator tuned at 300, 600, 900 Hz, etc., would work independently among each other as shown in Fig. 2(b), and large magnitude response can be obtained at the interested control frequency, while at other frequency spectrum, the magnitude is below 0 dB and no effective control can be implemented.

Therefore, it can be found out that for each single resonant regulator in (5), the bandwidth parameter ω_c can be introduced as

$$\frac{s}{s^2+\omega_c s+\omega_n^2} = \frac{1}{\dfrac{1}{\dfrac{s}{s^2+\omega_n^2}} + \omega_c}. \tag{6a}$$

Considering that each single resonant regulator in (5) would work independently and do not interfere with each other (that is high magnitude response around 30–50 dB at the interested control frequency of 300, 600, and 900 Hz, while large attenuation of magnitude response below 0 dB at the noninterested control frequency spectrum as shown in Fig. 2), then the following equation can be obtained based on (6a) from the perspective of mathematical approximation (which can be explained as, the sum of reciprocal of each single resonant regulator would be approximate to the reciprocal of sum of the resonant regulators):

$$\begin{aligned}\sum_{n=1}^{\infty}\frac{s}{s^2+\omega_c s+\omega_n^2} &= \sum_{n=1}^{\infty}\frac{1}{\dfrac{1}{\dfrac{s}{s^2+\omega_n^2}} + \omega_c} \\ & \qquad G_{\mathrm{rcs\_b}}(s) \qquad\qquad \uparrow \\ & \qquad \downarrow \qquad\qquad G_{\mathrm{rcs\_a}}(s) \\ &\approx \frac{1}{\dfrac{1}{\sum\limits_{n=1}^{\infty}\dfrac{s}{s^2+\omega_n^2}} + \omega_c} = \frac{1}{\frac{1}{\mathrm{RESO}} + \omega_c} \\ &= \frac{1}{\dfrac{2k_{\mathrm{rc}}}{T_0}\dfrac{1}{G_{\mathrm{rcs}}(s) + \dfrac{k_{\mathrm{rc}}}{2} - \dfrac{k_{\mathrm{rc}}}{T_0}\dfrac{1}{s}} + \omega_c}\end{aligned} \tag{6b}$$

where ω_c is the bandwidth in the proposed BRC regulator, the $G_{\mathrm{rcs\_a}}(s)$ represents the expression before mathematical approximation, and the $G_{\mathrm{rcs\_b}}(s)$ represents the expression after mathematical approximation, and the "$\approx$" is adopted to present the mathematical approximation of "the sum of reciprocal of each single resonant regulator would be approximate to the reciprocal of sum of the resonant regulators."

It should be noted that the accuracy of the proposed mathematical approximation between $G_{\mathrm{rcs\_a}}(s)$ and $G_{\mathrm{rcs\_b}}(s)$ can be validated based on Fig. 3. As shown in Fig. 3(a), the magnitude response of both $G_{\mathrm{rcs\_a}}(s)$ and $G_{\mathrm{rcs\_b}}(s)$ would be the same at the interested control frequency of 300, 600, and 900 Hz, while only tiny difference can be observed at the noninterested control frequency, which can be seen from Fig. 3(b), that is, –50 dB of $G_{\mathrm{rcs\_a}}(s)$ and -70 dB at $G_{\mathrm{rcs\_b}}(s)$ at 458 Hz. Besides, the frequency response of both $G_{\mathrm{rcs\_a}}(s)$ and $G_{\mathrm{rcs\_b}}(s)$ would also be the same at 300, 600, and 900 Hz, while tiny difference of phase response can be found around 458 Hz as shown in Fig. 3(b). Thus, it can be concluded that the proposed mathematical approximation between $G_{\mathrm{rcs\_a}}(s)$ and $G_{\mathrm{rcs\_b}}(s)$ in (6b) is sufficiently accurate to ensure the same magnitude and phase response of these two expressions at the interested control frequency; therefore, the satisfactory control performance using the expression $G_{\mathrm{rcs\_b}}(s)$ after approximation can be guaranteed.

Therefore, the BRC regulator with bandwidth parameter in the continuous domain can be approximately obtained based on (6b) as

$$\begin{aligned}G_{\mathrm{brcs}}(s) &= \frac{k_{\mathrm{brc}}}{\dfrac{1}{\mathrm{RESO}} + \omega_c} \\ &= \frac{k_{\mathrm{brc}}}{\dfrac{2}{T_0}\dfrac{1}{\dfrac{e^{-sT_0}}{1-e^{-sT_0}} + \dfrac{1}{2} - \dfrac{1}{T_0 s}} + \omega_c}\end{aligned} \tag{7}$$

where k_{brc} is the gain parameter of BRC regulator to adjust the magnitude response at the interested frequency.

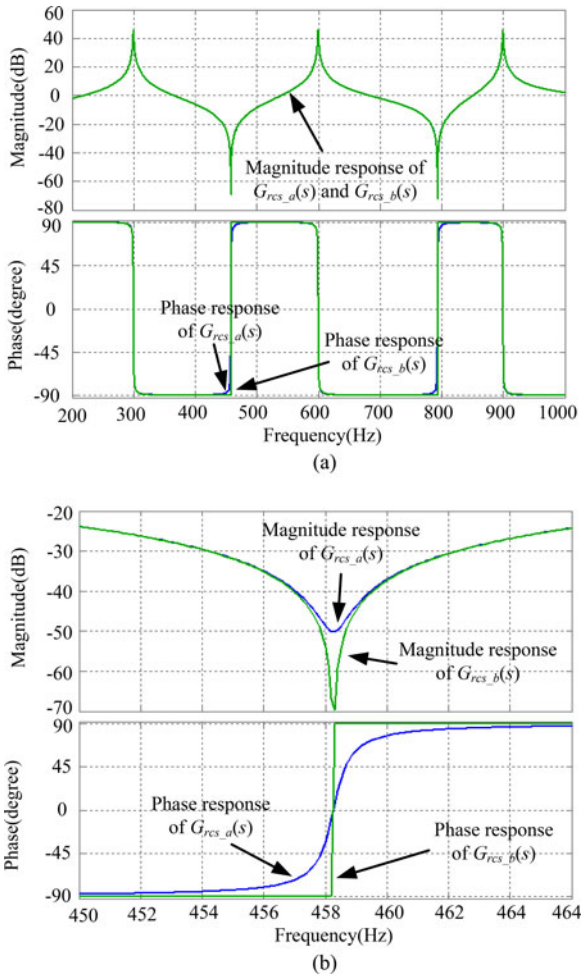

Fig. 3. Bode diagram of expression before and after the mathematical approximation in (6b), the $G_{\mathrm{rcs\_}a}(s)$ represents the expression before mathematical approximation, and the $G_{\mathrm{rcs\_}b}(s)$ represents the expression after mathematical approximation ($\omega_c = 10$ rad/s, the resonant gain parameter of both expression is set 1000).

Based on the mathematical deduction in (5)–(7), the BRC regulator in the continuous domain can be obtained; naturally, the same mathematical deduction can be implemented in the conventional RC regulator in the discrete domain as following. By replacing the RC regulator in continuous domain with the RC regulator expression (4a) and (4b) in discrete domain, and replacing abnormal PI part in continuous domain with the one in discrete domain (using the discretization method of bilinear), the BRC regulator in discrete domain can be finally expressed as

$$G_{\mathrm{brc}z}(z) = \frac{k_{\mathrm{brc}}}{\dfrac{2}{T_0}\dfrac{1}{\dfrac{Q(z)z^{-N}}{1-Q(z)z^{-N}} + \dfrac{1}{2} - \dfrac{T_s}{T_0}\dfrac{z}{z-1}} + \omega_c}. \quad (8)$$

It can be observed from (8) that the abnormal PI part in the conventional RC regulator can be removed in the BRC regulator, and the bandwidth ω_c can be also introduced. However, these modifications make the expression of BRC regulator $G_{\mathrm{brc}}(z)$ more complicated than the conventional RC regulator. Since the stator current control error dc component can be eliminated by the high-pass filter in the proposed control strategy shown in Fig. 1, thus keeping the abnormal PI part would have no negative influence on the control performance. Therefore, the BRC regulator with abnormal PI part can be presented with simpler expression as

$$\begin{aligned} G_{\mathrm{brc}z\mathrm{PI}}(z) &= \frac{k_{\mathrm{rcb}}}{\dfrac{2}{T_0}\dfrac{1}{\dfrac{Q(z)z^{-N}}{1-Q(z)z^{-N}}} + \omega_c} \\ &= \frac{k_{rcb}T_0Q(z)z^{-N}}{2\left(1-Q(z)z^{-N}\right) + \omega_c T_0 Q(z)z^{-N}}. \end{aligned} \quad (9)$$

For the sake of simplicity in the following discussion, only the BRC regulator with abnormal PI regulator $G_{\mathrm{brcPI}}(z)$ in (9) would be mentioned. Moreover, it can also be found that when $\omega_c = 0$ rad/s, (9) is the same as the conventional RC regulator in (4a).

It should be noted that the bandwidth ω_c can be adjusted flexibly. Fig. 4 gives out the bode diagram of conventional RC regulator $G_{\mathrm{rc}z}(z)$ in (4a) and (4b) and the proposed BRC regulator $G_{\mathrm{brcPI}}(z)$ in (9), with the parameters of $Q(z) = 2/3 + 1/3^{*}z^{-1}$, $T_0 = 1/300$ s and $N = 33$; $k_{\mathrm{brc}} = 250$ when $\omega_c = 0$ rad/s; $k_{\mathrm{brc}} = 460$ when $\omega_c = 2$ rad/s; $k_{\mathrm{brc}} = 820$ when $\omega_c = 5$ rad/s; $k_{\mathrm{brc}} = 1300$ when $\omega_c = 10$ rad/s. The gain parameter k_{brc} in previous cases is determined on the basis of equal magnitude response of 40 dB at 300 Hz when different bandwidth parameter is employed.

As can be observed from Fig. 4(a), the conventional RC regulator would have the large gain of 53 dB for the dc component due to the existence of abnormal PI part, while the proposed BRC regulator with PI part in the case of bandwidth $\omega_c = 2, 5, 10$ rad/s as given in (9) would also have the large gain of 40 dB for the dc component. Due to the introduction of high-pass filter in the stator current control loop as described in Fig. 1, the abnormal PI part would bring no negative influence to the control performance. Moreover, it can also be found out from Fig. 4(a) that the satisfactory magnitude response of high gain at the interested frequency can be obtained for both conventional RC regulator and the proposed BRC regulator.

Fig. 4(b) gives out the bode diagram of conventional RC and proposed BRC regulators within the frequency spectrum of 200–1000 Hz. As shown in Fig. 4(b), the large gain can be obtained, i.e., 40 dB for conventional RC and BRC with $\omega_c = 2, 5, 10$ rad/s at 300 Hz; 28 dB for conventional RC and 32–36 dB of BRC with $\omega_c = 2, 5, 10$ rad/s at 600 Hz; 21 dB for conventional RC and 26–33 dB of BRC with $\omega_c = 2, 5, 10$ rad/s at 900 Hz. Besides, the same phase response of 0° at 300, 600, and 900 Hz for both conventional RC regulator and proposed BRC regulator can be achieved. Therefore, it can be concluded that the proposed BRC regulator would have better control performance than the conventional RC regulator when the grid works under normal frequency of 50 Hz due to the higher magnitude response of BRC regulator at the interested frequency.

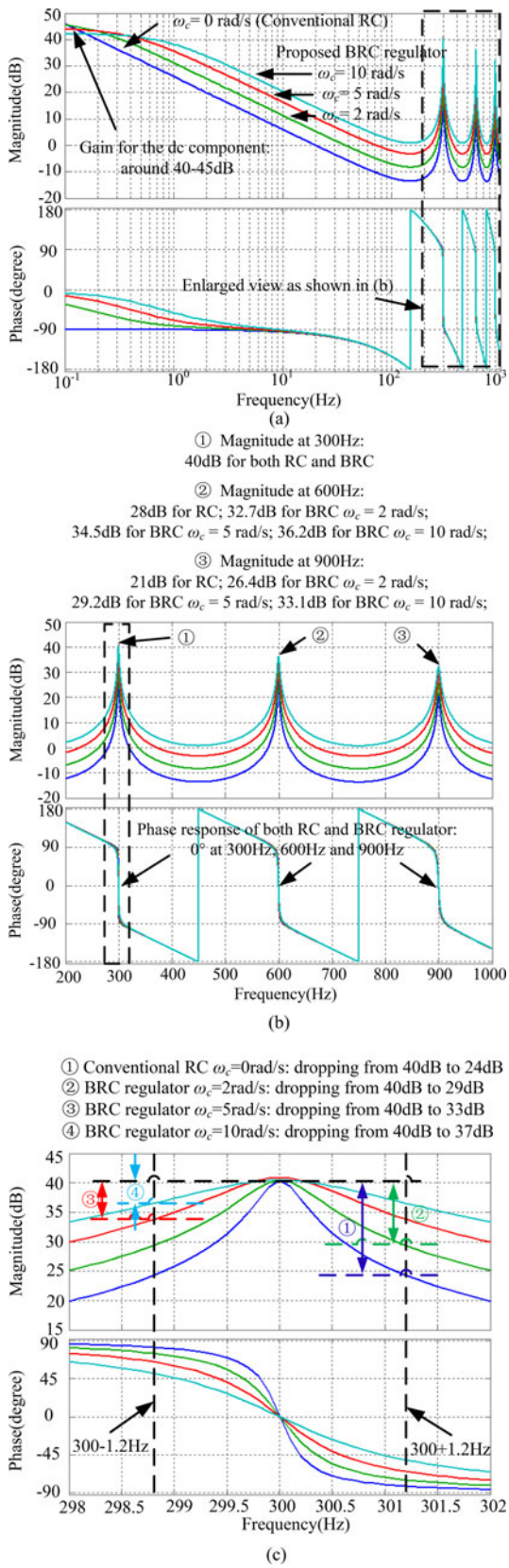

Fig. 4. Bode diagram of the conventional RC regulator $G_{\mathrm{rcz}}(z)$ and the proposed BRC regulator $G_{\mathrm{brcPI}}(z)$ ($Q(z) = 2/3 + 1/3^{*}z^{-1}, T_0 = 1/300$ s and $N = 33$; $k_{\mathrm{brc}} = 250$ when $\omega_c = 0$ rad/s; $k_{\mathrm{brc}} = 460$ when $\omega_c = 2$ rad/s; $k_{\mathrm{brc}} = 820$ when $\omega_c = 5$ rad/s; $k_{\mathrm{brc}} = 1300$ when $\omega_c = 10$ rad/s).

Fig. 4(c) gives out the bode diagram of conventional RC and proposed BRC regulators within the frequency of 298–302 Hz, when grid frequency deviation of 50 ± 0.2 Hz (i.e., 300 ± 1.2 Hz) happens. As shown in Fig. 4(c), the conventional RC regulator and proposed BRC regulator with different bandwidth would have different response when the grid frequency deviation happens. For the conventional RC regulator ($\omega_c = 0$ rad/s), the magnitude response would drop from 40 to 24 dB, which would deteriorate the stator current harmonic suppression capability because of the larger steady-state control error, while the proposed BRC regulator with bandwidth $\omega_c = 2$ rad/s would have the magnitude response drop from 40 to 29 dB, and similarly from 40 to 33 dB with $\omega_c = 5$ rad/s, from 40 to 37 dB with $\omega_c = 10$ rad/s. Therefore, it can be found that when the bandwidth ω_c is introduced to the conventional RC regulator, the extent of magnitude response decreasing would become much smaller, that is 16 dB when no bandwidth, 11 dB when $\omega_c = 2$ rad/s, 7 dB when $\omega_c = 5$ rad/s, and 3 dB when $\omega_c = 10$ rad/s. Furthermore, the phase response at 300 Hz would also deviate from 0° when the grid frequency deviation happens. By comparing the four curves with different bandwidth, it can be found that when larger bandwidth is selected, the much smaller phase response changing can be observed, i.e., −55° to 55° when $\omega_c = 10$ rad/s, −65° to 65° when $\omega_c = 5$ rad/s, −75° to 75° when $\omega_c = 2$ rad/s, and −80° to 80° when $\omega_c = 0$ rad/s. As a result, the closed-loop control performance of stator current harmonic suppression would be comparatively less deteriorated when the larger bandwidth parameter is employed. Thus, it can be validated that the introduction of bandwidth in the proposed RBC regulator would be helpful to improve its robustness against grid frequency deviation from both the perspective of magnitude response and phase response, and the proposed BRC regulator would be more appropriate than the conventional RC regulator in the practical grid situation when grid frequency deviation occurs.

C. Closed-Loop Control Stability Analysis

As reported in the previous works [18]–[21], the RC regulator-based control system may always suffer the instability operation, and even results in the failure of the DFIG control target. It is critical to make sure that the proposed BRC stator current control would operate stably, so discussing the closed-loop control stability with different bandwidth ω_c and different gain parameter k_{brc} would be essential.

Fig. 5 shows the block diagram of proposed BRC-based DFIG control system for the stator current harmonic suppression. Since the BRC regulator is sensitive to the dc error component as described in Fig. 4(a), the high-pass filter is introduced to eliminate the dc error component in the stator feedback current I^{+}_{sdq}, then the stator current harmonic component $I^{+}_{\mathrm{sdq}H}$ is considered as the BRC regulator feedback.

According to [8], the DFIG transfer function from BRC regulator output to the stator current in the continuous domain can be deduced as

$$G_{\mathrm{plant}}(s) = \frac{L_m}{L_s}\frac{1}{R_r + s\sigma L_r}. \tag{10a}$$

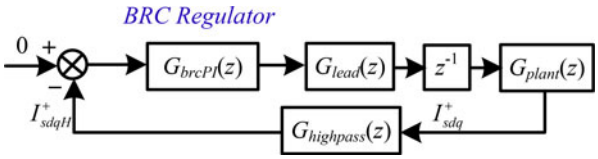

Fig. 5. Block diagram of the proposed BRC closed-loop control.

Based on (10a) and the discretization method of impulse invariant, the DFIG transfer function in the discrete domain can be presented as

$$G_{\text{plant}}(z) = \frac{T_s L_m}{\sigma L_s L_r} \frac{z}{z - e^{-T_s R_r/\sigma L_r}} \tag{10b}$$

where T_s is the sample period of 1e–4 s.

In order to avoid the BRC regulation on the fundamental component of stator current, a high-pass filter with the cutoff frequency of 10 Hz is introduced to remove the stator current control error dc component before feeding back to the BRC regulator

$$G_{\text{highpass}}(s) = \frac{s}{s+a} = \frac{s}{s+20\pi} \tag{11a}$$

where a is the cutoff frequency of 20π rad/s.

The discretization method of bilinearization is employed to obtain the high-pass filter in the discrete domain as

$$\begin{aligned} G_{\text{highpass}}(z) &= \frac{2z-2}{(2+aT_s)z-(2-aT_s)} \\ &= \frac{2z-2}{2.006z-1.994}. \end{aligned} \tag{11b}$$

According to Fig. 4, it can be found out that the BRC regulator would only introduced 0° for the 300, 600, and 900 Hz components, thus having no negative influence on the stator current control performance. Moreover, the high-pass filter would also introduce negligible phase delay of 1.9°, 0.95°, and 0.63° at 300, 600, and 900 Hz, respectively. Therefore, it can be concluded that the major control delay is caused by the control subject DFIG and the digital control delay of one sample period [24], [25], and the phase leading unit should be accurately designed to compensate these two delay units as

$$G_{\text{lead}}(z) = \frac{1}{G_{\text{plant}}(z)z^{-1}} = \frac{\sigma L_s L_r}{T_s L_m}\left(z - e^{-R_r/\sigma L_r}\right). \tag{12}$$

Based on (9)–(12) and Fig. 5, the control system transfer function can be deduced as

$$\begin{aligned} C_{cl-\text{lead}}(z) &= \frac{I_{\text{sdq}}(z)}{I^{\text{ref}}_{\text{sdq}}(z)} \\ &= \frac{G_{\text{brcPI}}(z)G_{\text{plant}}(z)z^{-1}G_{\text{lead}}(z)}{1+G_{\text{brcPI}}(z)G_{\text{plant}}(z)z^{-1}G_{\text{lead}}(z)G_{\text{highpass}}(z)}. \end{aligned} \tag{13}$$

Thus, according to (13), the transfer function of stator current from the reference to the error can be presented as

According to (14) shown in the bottom of page, in order to assure that the control system is stable, the following condition should be satisfied:

$$\left|\left(\left(1-\frac{\omega_c T_0}{2}\right) - \frac{k_{\text{brc}}T_0}{2}G_{\text{plant}}(e^{j\omega T_s})e^{-j\omega T_s} G_{\text{lead}}(e^{j\omega T_s})G_{\text{highpass}}(e^{j\omega T_s})\right) Q(e^{j\omega T_s})\right| < 1 \tag{15}$$

where $\omega = [20\pi, 10000\pi]$. It means that as ω increases, the system will be stable if $S(z)$ is confined within the unity circle. Since the proposed high-pass filter has the cutoff frequency of 10 Hz, the BRC-based stator current closed-loop control would not include the error component with the frequency lower than 10 Hz. Thus, the lower limit of the angular speed discussed in (15) is 20π rad/s, and the upper limit would be the Nyquist frequency of 5 kHz (10 000π rad/s) due to the sample frequency of 10 kHz.

Fig. 6 gives out the locus of the vector $S(z)$ with different BRC regulator bandwidth parameter $\omega_c = 2$, 5, 10 rad/s and $k_{\text{brc}} = 460$, 820, and 1300, respectively. As can be observed from Fig. 6, when certain k_{brc} is chosen, the different bandwidths of 2, 5, and 10 rad/s would have almost the same performance considering the closed-loop stability, as can be proved in Fig. 6. Moreover, when different gain parameter k_{rbc} is implemented, the locus curve would be much different, for instance, when the $k_{\text{brc}} = 460$ is chosen, the closed-loop operation would have overlarge stability margin due to its response within the range of 0.6; while $k_{\text{brc}} = 820$ is chosen, the closed-loop would have appropriate margin of within the range of 0.8, and the larger k_{brc} would be helpful to suppress the control error. However, when overlarge $k_{\text{brc}} = 1300$ is implemented, the locus goes out of the unity circle, and instability operation would be a consequence.

Thus, it can be concluded from Fig. 6 that: 1) The bandwidth parameter ω_c would have negligible influence on the closed-loop operation stability; thus, adjusting the bandwidth flexibly according to different grid frequency deviation condition would

$$\begin{aligned} \frac{I^{\text{err}}_{\text{sdq}}(z)}{I^{\text{ref}}_{\text{sdq}}(z)} &= 1 - \frac{I_{\text{sdq}}(z)}{I^{\text{ref}}_{\text{sdq}}(z)} \\ &= \frac{1+G_{\text{brcPI}}(z)G_{\text{plant}}(z)z^{-1}G_{\text{lead}}(z)\left(G_{\text{highpass}}(z)-1\right)}{1+G_{\text{brcPI}}(z)G_{\text{plant}}(z)z^{-1}G_{_{\text{lead}}}(z)G_{\text{highpass}}(z)} \\ &= \frac{\left(1+G_{\text{brcPI}}(z)G_{\text{plant}}(z)z^{-1}G_{\text{lead}}(z)\left(G_{\text{highpass}}(z)-1\right)\right)\left(1+\left(\frac{\omega_c T_0}{2}-1\right)Q(z)z^{-N}\right)}{1-\left(\left(1-\frac{\omega_c T_0}{2}\right)-\frac{k_{\text{brc}}T_0}{2}G_{\text{plant}}(z)z^{-1}G_{\text{lead}}(z)G_{\text{highpass}}(z)\right)Q(z)z^{-N}}. \end{aligned} \tag{14}$$

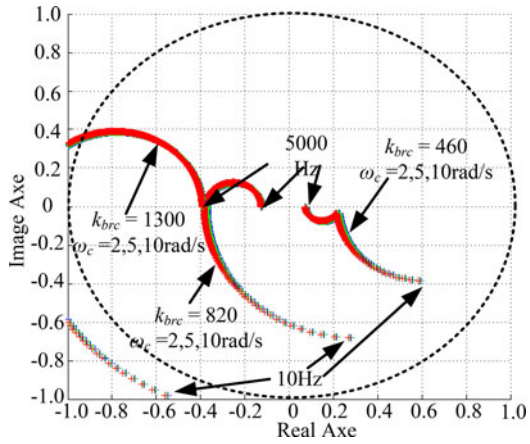

Fig. 6. Locus of the vector $S(z)$ with different bandwidth from 2, 5, and 10 rad/s, and $k_{\rm brc} = 460, 820, 1300$, $z = e^{j\omega T s}$, $(\omega = [20\pi, 10000\pi])$.

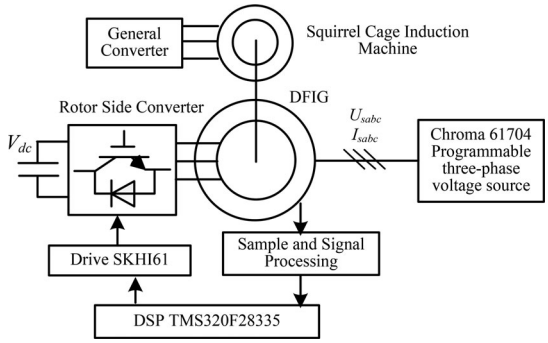

Fig. 7. Block diagram of the experiment system.

be applicable in the practical situation; 2) the closed-loop stability is mainly determined by the gain parameter $k_{\rm brc}$, and larger $k_{\rm brc}$ means better steady-state tracking accuracy, but also means smaller stability margin. Therefore, an appropriate selection of $k_{\rm brc}$ with the compromise between closed-loop operation stability and steady-state tracking accuracy should be carefully considered.

Furthermore, as proved in Fig. 6, the stable operation of BRC-based stator current control is relatively easy to achieve in the practical situation; thus, no low-pass filter or coefficient smaller than 1.0, as adopted in [12]–[21] to improve the closed-loop operation stability, is needed in this paper.

V. Experimental Validation

A. Experimental Setup

Experiment system was developed on a laboratory prototype of 1 kW DFIG system as shown in Fig. 7, in which the DFIG is driven by a squirrel cage induction machine as the wind turbine. The Chroma 61704 programmable three-phase voltage source is set up to simulate the harmonic distorted power grid. In the experiment, grid voltage 5th-, 7th-, 11th-, 13th-, 17th-, and 19th-order harmonic components are set as 2.98%, 2.91%, 2.68%, 2.57%, 2.37%, and 2.18%, respectively. The rotor speed is initially set to 800 r/min, while the synchronous speed is 1000 r/min.

TABLE I
Parameters of Experiment DFIG System

Rated power	1 kW	DFIG mutual inductance L_m	90.1 mH
Grid voltage (RMS of phase to phase)	110 V	DFIG stator leakage inductance $L_{\sigma s}$	3.0 mH
Stator/rotor turns ratio	0.33	DFIG rotor leakage inductance $L_{\sigma r}$	3.0 mH
Stator resistance R_s	1.01 Ω	DFIG pole pairs	3
Rotor resistance R_r	0.88 Ω	DC-link voltage $V_{\rm dc}$	200 V
Sample frequency	10k Hz	Switching frequency	10 kHz

The grid-side converter working under harmonic distorted grid voltage would produce dc-link voltage fluctuation of 300, 600, 900 Hz, etc.; this fluctuations would have same fluctuation frequency as the stator current harmonic components in the synchronous dq^+ frame (that is, 300, 600, 900, etc.). Therefore, the proposed BRC strategy for the DFIG rotor-side converter can be similarly implemented in the grid-side converter; that is, first, in the outer control loop, the closed-loop dc-link voltage 300, 600, 900 Hz fluctuation RC control would produce the inner control loop reference, which is the reference for the grid-side converter current; then, in the inner control loop, the grid-side converter current can be accurately regulated according to the reference by the closed-loop grid-side converter current RC control. Finally, the dc-link voltage fluctuation of 300, 600, 900 Hz, etc., can be well eliminated, and smooth dc-link voltage can be guaranteed. However, in order to simplify the paper contents and highlight the DFIG control performance with the proposed BRC strategy, the control of grid-side converter is neglected here, and the dc power supply is adopted in the experiment to replace the grid-side converter to provide stable dc-link voltage of 200 V.

The proposed BRC strategy is implemented on the TI DSP TMS320F28335. The sampling frequency is 10 kHz, and the IGBT switching frequency is 10 kHz. The experimental waveforms are acquired by a YOKOGAWA DL750 scope recorder; the harmonic analysis is conducted by a FLUKE NORMA 5000 power analyzer. Parameters of the tested DFIG system are listed in Table I. The photograph of experimental setup can be found in Fig. 8.

B. Experimental Results

Fig. 9 shows the experimental result of DFIG under both low- and high-order harmonic distorted grid voltage condition with frequency of 50 Hz when BRC control of stator current is disabled and the PI control of rotor current is enabled. Due to the heavy grid voltage distortion with abundant low- and high-order harmonic sequences, the severely distorted DFIG stator current would occur as a consequence, i.e., harmonic components of 5.63% 5th, 4.14% 7th, 2.57% 11th, 1.99% 13th, 1.97% 17th, and 1.86% 19th sequence, as shown in Table II. Thus, it can be seen

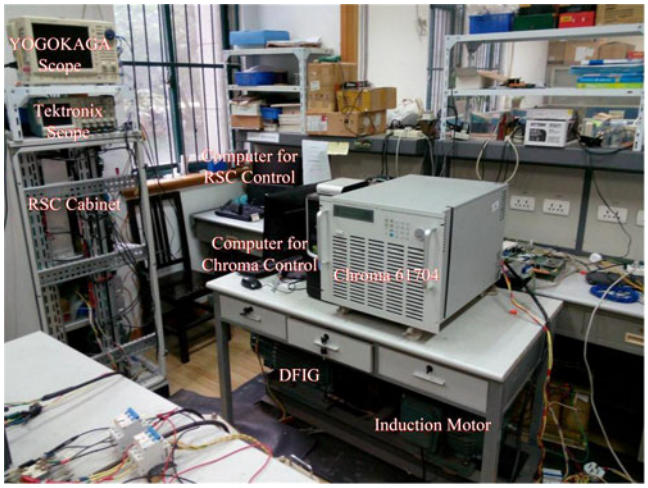

Fig. 8. Photograph of experiment setup.

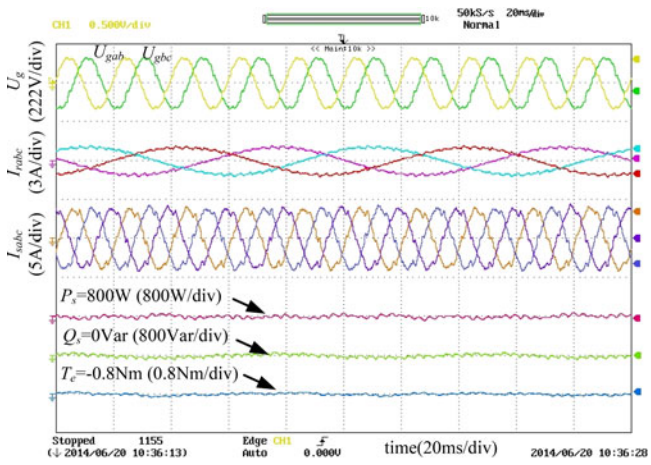

Fig. 9. Experimental result of DFIG under generalized harmonic distorted grid voltage condition with frequency of 50 Hz when BRC control of stator current is disabled and the PI control of rotor current is enabled.

TABLE II
EXPERIMENT RESULT ANALYSIS DATA

	Grid voltage	BRC is disabled	50 Hz, BRC ω_c = 10 rad/s	49.8 Hz, conventional RC	49.8 Hz, BRC ω_c = 10 rad/s
5th harmonic	2.98%	5.63%	0.81%	1.29%	0.82%
7th harmonic	2.91%	4.14%	0.72%	0.96%	0.70%
11th harmonic	2.68%	2.57%	0.91%	1.40%	1.15%
13th harmonic	2.57%	1.99%	0.82%	1.22%	0.91%
17th harmonic	2.37%	1.97%	0.93%	1.15%	1.01%
19th harmonic	2.18%	1.86%	0.77%	1.00%	0.88%

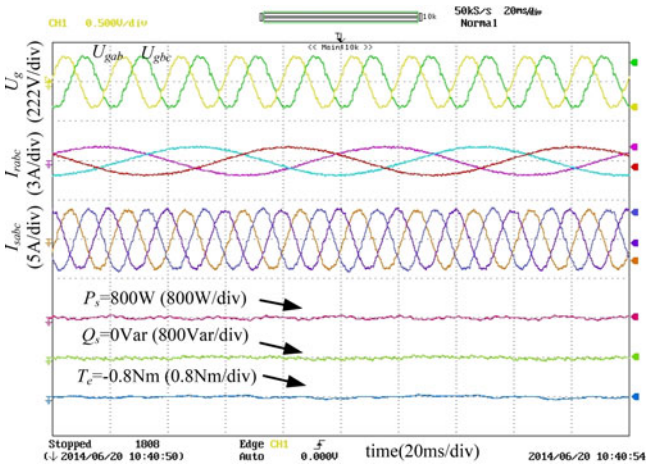

Fig. 10. Experimental result of DFIG under generalized harmonic distorted grid voltage condition with frequency of 50 Hz when BRC control is enabled and bandwidth $\omega_c - 10\,\mathrm{rad/s}$.

that DFIG operation performance would be severely jeopardized if the harmonic suppression strategy is not implemented.

Fig. 10 shows the experimental result of DFIG performance under the generalized harmonic distorted grid voltage condition with frequency of 50 Hz when BRC control is enabled and bandwidth ω_c is chosen as 10 rad/s. As can be seen, once the effective BRC regulator is enabled, the stator current harmonic components can be efficiently suppressed to 0.81% 5th sequence, 0.72% 7th sequence, 0.91% 11th sequence, 0.82% 13th sequence, 0.93% 17th sequence, and 0.77% 19th sequence, as shown in Table II. Therefore, it can be proved that the proposed BRC regulator with bandwidth of 10 rad/s would work effectively under the normal grid voltage frequency of 50 Hz, and the sinusoidal DFIG stator current can be achieved in the steady-state performance due to the excellent BRC regulator harmonic components suppression capability.

Fig. 11 shows the experimental result of DFIG under harmonic distorted grid voltage condition with frequency of 49.8 Hz when (a) conventional RC regulator or (b) BRC regulator with bandwidth $\omega_c = 10$ rad/s is proposed. As can be seen from Table II, when conventional RC regulator is adopted in Fig. 11(a), the stator current harmonic distortion would include 1.29% 5th, 0.96% 7th, 1.40% 11th, 1.22% 13th, 1.15% 17th, and 1.00% 19th sequence; while the BRC regulator with $\omega_c = 10$ rad/s is adopted in Fig. 11(b), the stator current harmonic distortion would include 0.82% 5th, 0.70% 7th, 1.15% 11th, 0.91% 13th, 1.01% 17th, and 0.88% 19th sequence. Thus, it can be found out from Table II that, compared with the steady-state performance under normal frequency 50 Hz, the steady-state performance with conventional RC regulator and BRC regulator under grid frequency deviation of 49.8 Hz would become worse. Moreover, it can also be validated that due to the introduction of bandwidth in the BRC regulator, the BRC regulator would have larger magnitude response at the deviated control frequency; thus, the better stator current harmonic components suppression of BRC regulator than that of conventional RC regulator can be guaranteed.

Fig. 12 shows the experimental result of DFIG output active power stepping under generalized harmonic distorted grid voltage condition with frequency of 49.8 Hz using BRC regulator with bandwidth $\omega_c = 10$ rad/s. The effective control of rotor

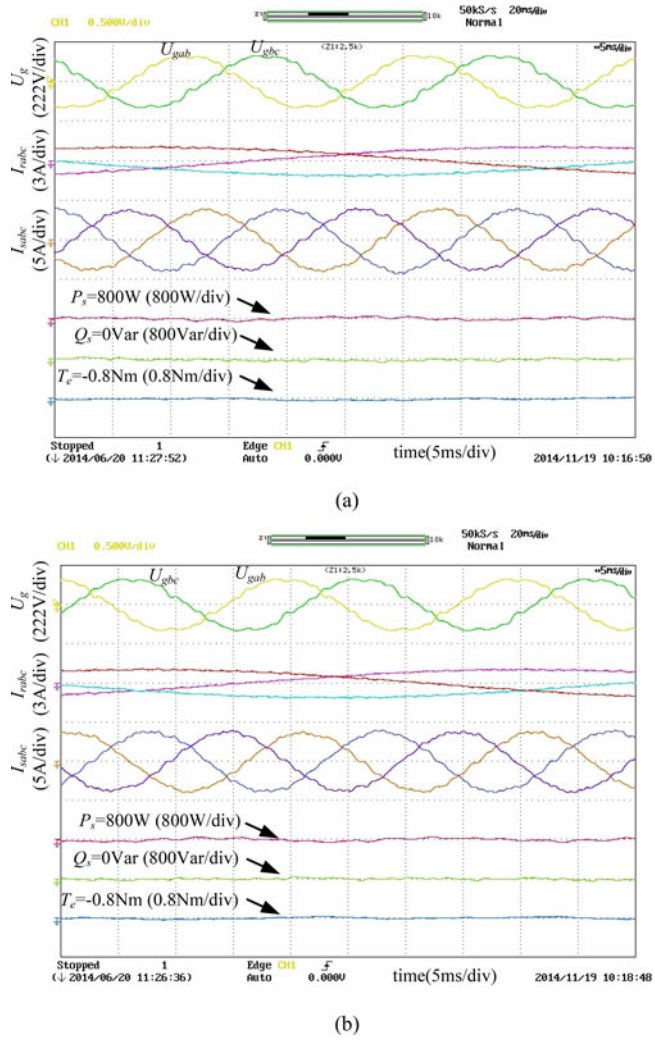

Fig. 11. Experimental result of DFIG under generalized harmonic distorted grid voltage condition with frequency of 49.8 Hz when (a) conventional RC regulator or (b) BRC regulator with bandwidth $\omega_c = 10\,\mathrm{rad/s}$ is proposed.

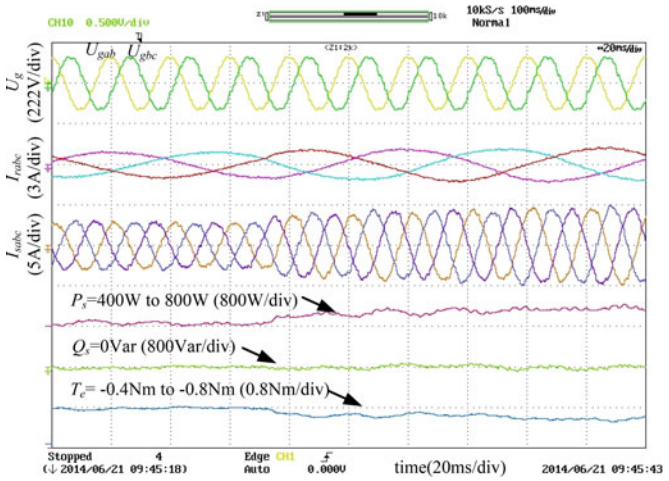

Fig. 12. Experimental result of DFIG output active power stepping under generalized harmonic distorted grid voltage condition with frequency of 49.8 Hz using BRC regulator with bandwidth $\omega_c = 10\,\mathrm{rad/s}$.

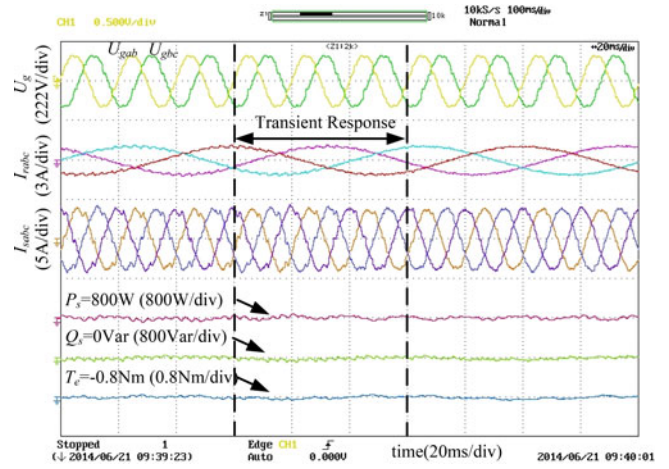

Fig. 13. Experimental result of DFIG transient response under generalized distorted grid voltage state when BRC regulator with bandwidth $\omega_c = 10\,\mathrm{rad/s}$ is enabled.

current PI closed-loop control is capable of achieving smooth transient response of DFIG stator active power stepping around 80 ms. Moreover, the DFIG stator current is able to maintain sinusoidal during the active power stepping process, and these experimental results prove that the proposed BRC control of stator current harmonic components can be implemented in the practical situation.

Fig. 13 shows experimental result of DFIG transient response under generalized distorted grid voltage state when BRC regulator with bandwidth $\omega_c = 10$ rad/s is enabled. The DFIG stator current contains heavily distorted harmonic components when BRC is disabled, while once the BRC regulator is enabled, the stator current harmonic components can be successfully restrained within around 60 ms; these experimental results prove that the proposed BRC regulator is applicable in the practical situation.

VI. Conclusion

The paper presents the control strategy of stator current harmonic distortion suppression for DFIG based on BRC regulator under generalized harmonic grid voltage. Compared with conventional RC regulator, the proposed BRC regulator can widen the effective control frequency spectrum by enlarging the magnitude response near the control frequency with the introduction of bandwidth parameter; thus, the BRC regulator would have stronger robustness against grid frequency deviation, and the better steady-state stator current harmonic components suppression can be assured. Furthermore, the closed-loop operation stability of the BRC based control system is mainly determined by the BRC regulator gain parameter, while bandwidth parameter would have negligible influence on the control stability.

References

[1] National Grid Transco, Appendix 1. (Feb. 2004). *Extracts from the Grid Code—Connection Conditions* [Online]. Available: http://www. national-grid.com

[2] *IEEE Recommended Practices and Requirements for Harmonic Control in Electrical Power Systems*, IEEE Standard 519-1992, 1993.

[3] J. Hu, H. Nian, H. Xu, and Y. He, "Dynamic modeling and improved control of DFIG under distorted grid voltage conditions," *IEEE Trans. Energy Convers.*, vol. 26, no. 1, pp. 163–175, Mar. 2011.
[4] J. Hu, H. Xu, and Y. He, "Coordinated control of DFIG's RSC and GSC under generalized unbalanced and distorted grid voltage conditions," *IEEE Trans. Ind. Electron.*, vol. 60, no. 7, pp. 2808–2819, Jul. 2013.
[5] H. Xu, J. Hu, and Y. He, "Integrated modeling and enhanced control of DFIG under unbalanced and distorted grid voltage conditions," *IEEE Trans. Energy Convers.*, vol. 27, no. 3, pp. 725–736, Jul. 2012.
[6] V.-T. Phan and H.-H. Lee, "Control strategy for harmonic elimination in stand-alone DFIG applications with nonlinear loads," *IEEE Trans. Power Electron.*, vol. 26, no. 9, pp. 2662–2675, Sep. 2011.
[7] H. Xu, J. Hu, and Y. He, "Operation of wind-turbine-driven DFIG systems under distorted grid voltage conditions: Analysis and experimental validations," *IEEE Trans. Power Electron.*, vol. 27, no. 5, pp. 2354–2366, May 2012.
[8] H. Nian and Y. Song, "Direct power control of doubly fed induction generator under distorted grid voltage," *IEEE Trans. Power Electron.*, vol. 29, no. 2, pp. 894–905, Feb. 2014.
[9] C. Liu, F. Blaabjerg, W. Chen, and D. Xu, "Stator current harmonic control with resonant controller for doubly fed induction generator," *IEEE Trans. Power Electron.*, vol. 27, no. 7, pp. 3207–3220, Jul. 2012.
[10] X. Wang, F. Blaabjerg, and Z. Chen, "Autonomous control of inverter-interfaced distributed generation units for harmonic current filtering and resonance damping in an islanded microgrid," *IEEE Trans. Ind. Appl.*, vol. 50, no. 1, pp. 452–461, Jan./Feb. 2014.
[11] A. G. Yepes, F. D. Freijedo, J. Doval-Gandoy, O. López, J. Malvar, and P. Fernandez-Comesaña, "Effects of discretization methods on the performance of resonant controllers," *IEEE Trans. Power Electron.*, vol. 25, no. 7, pp. 1692–1712, Jul. 2010.
[12] D. Chen, J. Zhang, and Z. Qian, "Research on fast transient and $6n \pm 1$ harmonics suppressing repetitive control scheme for three-phase grid-connected inverters," *IET Power Electron*., vol. 6, no. 3, pp. 601–610, 2013.
[13] F. Wei, X. Zhang, D. M. Vilathgamuwa, S. S. Choi, and S. Wang, "Mitigation of distorted and unbalanced stator voltage of stand-alone doubly fed induction generators using repetitive control technique," *IET Electron Power Appl.*, vol. 7, no. 8, pp. 654–663, 2013.
[14] K. Zhou, D. Wang, B. Zhang, and Y. Wang, "Plug-in dual-mode-structure repetitive controller for CVCF PWM inverters," *IEEE Trans. Ind. Electron.*, vol. 56, no. 3, pp. 784–791, Mar. 2009.
[15] Q. Zhong and T. Hornik, "Cascaded current–voltage control to improve the power quality for a grid-connected inverter with a local load," *IEEE Trans. Ind. Electron.*, vol. 60, no. 4, pp. 1344–1355, Apr. 2013.
[16] Q. Trinh and H. Lee, "An enhanced grid current compensator for grid-connected distributed generation under nonlinear loads and grid voltage distortions," *IEEE Trans. Ind. Electron.*, vol. 61, no. 12, pp. 6528–6537, Dec. 2014.
[17] E. Kurniawan, Z. Cao, and Z. Man, "Design of robust repetitive control with time-varying sampling periods," *IEEE Trans. Ind. Electron.*, vol. 61, no. 6, pp. 2834–2841, Jun. 2014.
[18] W. Lu, K. Zhou, D. Wang, and M. Cheng, "A generic digital nk±m order harmonic repetitive control scheme for PWM converters," *IEEE Trans. Ind. Electron.*, vol. 61, no. 3, pp. 1516–1527, Mar. 2014.
[19] B. Zhang, K. Zhou, and D. Wang, "Multirate repetitive control for PWM DC/AC converters," *IEEE Trans. Ind. Electron.*, vol. 61, no. 6, pp. 2883–2890, Jun. 2014.
[20] Y. Yang, K. Zhou, M. Cheng, and B. Zhang, "Phase compensation multiresonant control of CVCF PWM converters," *IEEE Trans. Power Electron.*, vol. 28, no. 8, pp. 3923–3930, Aug. 2013.
[21] W. Lu, K. Zhou, D. Wang, and M. Cheng, "A general parallel structure repetitive control scheme for multiphase DC–AC PWM converters," *IEEE Trans. Power Electron.*, vol. 28, no. 8, pp. 3980–3987, Aug. 2013.
[22] *Quality of Electric Energy Supply: Permissible Deviation of Frequency for Power System*, GB/T 15945-1995, 1995 (in Chinese).
[23] D. Chen, J. Zhang, and Z. Qian, "An improved repetitive control scheme for grid-connected inverter with frequency-adaptive capability," *IEEE Trans. Ind. Electron.*, vol. 60, no. 2, pp. 814–823, Feb. 2013.
[24] M. Castilla, J. Miret, J. Matas, L. García de Vicuña, and J. M. Guerrero, "Control design guidelines for single-phase grid-connected photovoltaic inverters with damped resonant harmonic compensators," *IEEE Trans. Ind. Electron.*, vol. 56, no. 11, pp. 4492–4501, Nov. 2009.
[25] Z. Li, Y. Li, P. Wang, H. Zhu, C. Liu, and F. Gao, "Single-loop digital control of high-power 400-Hz ground power unit for airplanes," *IEEE Trans. Ind. Electron.*, vol. 57, no. 2, pp. 532–543, Feb. 2010.

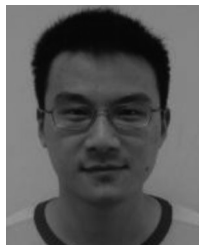

Yipeng Song (S'14) was born in Hangzhou, China. He received the B.Sc. degree from the College of Electrical Engineering, Zhejiang University, Hangzhou, in July 2010, where he is currently working toward the Ph.D. degree.

His current research interests include motor control with power electronics devices in renewable-energy conversion, particularly the control and operation of doubly fed induction generators for wind power generation under adverse grid condition.

Heng Nian (M'09–SM'14) received the B.Eng. and M.Eng. degrees from the Hefei University of Technology, Hefei, China, and the Ph.D. degree from Zhejiang University, Hangzhou, China, in 1999, 2002, and 2005, respectively, all in electrical engineering.

From 2005 to 2007, he was as a Postdoctoral Researcher with the College of Electrical Engineering, Zhejiang University, where he has been an Associate Professor since 2007. His current research interests include the optimal design and operation control for the wind power generation system.